1-6-2019

Unusual pressure-induced electronic structure evolution in organometal halide perovskite predicted from first-principles

Fei Wang
Zhengzhou University

Mengping Tan
Zhengzhou University

Chong Li
Zhengzhou University

Chunyao Niu
Zhengzhou University

Xin Zhao
Iowa State University and Ames Laboratory

Unusual pressure-induced electronic structure evolution in organometal halide perovskite predicted from first-principles

Abstract
Pressure has been demonstrated to be an effective parameter to alter the atomic and electronic structures of materials. By using the first-principles calculations based on density functional theory (DFT), we systematically investigated the changes in the atomic and electronic structures of the cubic MAPbI(3) phase under pressures. It is found that the band gap of the compressed cubic MAPbI(3) structure exhibits a remarkable redshift to 1.114/1.380 eV in DFT/HSE-SOC calculation under a mild pressure of 2.772 GPa, and subsequently shows a widening at higher pressures until similar to 20 GPa. As the pressure further increases, the band gap closes at similar to 80 GPa. Detailed structural and electronic characteristic analyses indicate that the band gap of the cubic MAPbI(3) structure is determined by two competing effects: the lattice contraction decreases its band gap while the PbI6 octahedral filling increases it. Given that, pressure can be a powerful tool to help understanding the optoelectronic properties of perovskite materials.

Keywords
Organometal halide perovskite, Pressure, Electronic structure, Density functional theory

Disciplines
Materials Science and Engineering

Unusual pressure-induced electronic structure evolution in organometal halide perovskite predicted from first-principles

Fei Wang[a,*], Mengping Tan[a], Chong Li[a], Chunyao Niu[a], Xin Zhao[b,**]

[a] International Laboratory for Quantum Functional Materials of Henan, and School of Physics and Engineering, Zhengzhou University, Zhengzhou, Henan, 450001, China

[b] Ames Laboratory, US DOE and Department of Physics and Astronomy, Iowa State University, Ames, IA, 50011, USA

Abstract

Pressure has been demonstrated to be an effective parameter to alter the atomic and electronic structures of materials. By using the first-principles calculations based on density functional theory (DFT), we systematically investigated the changes in the atomic and electronic structures of the cubic $MAPbI_3$ phase under pressures. It is found that the band gap of the compressed cubic $MAPbI_3$ structure exhibits a remarkable redshift to 1.114/1.380 eV in DFT/HSE-SOC calculation under a mild pressure of 2.772 GPa, and subsequently shows a widening at higher pressures until ~20 GPa. As the pressure further increases, the band gap closes at ~80 GPa. Detailed structural and electronic characteristic analyses indicate that the band gap of the cubic $MAPbI_3$ structure is determined by two competing effects: the lattice contraction decreases its band gap while the PbI_6 octahedral tilting increases it. Given that, pressure can be a powerful tool to help understanding the optoelectronic properties of perovskite materials.

Keywords: Organometal halide perovskite; Pressure; Electronic structure; Density functional theory

1. Introduction

Solar cells based on the methylammonium (MA) lead halide perovskites have been rapidly developed in the past few years, with the power conversion efficiency increasing from 3.8% [1] in 2009 to 23.3% in 2018 [2]. Compared with other solar cell photovoltaic absorbers, the organometalhalide perovskites are generating great excitement due to their high absorption coefficient, high yield of charge carriers following photo-excitation, and excellent charge transport properties. With considerable efforts devoted from both the theoretical and experimental sides, substantial progress has been made in understanding the electronic structure of $MAPbI_3$ and the dynamics of photo-excited charge carriers in $MAPbI_3$ [3-7], which clearly indicates that band-gap modification plays an important role in improving the optoelectronic

properties of $MAPbI_3$. In particular, it has been tempting to further narrow the band gap of $MAPbI_3$ to approach the Schockley-Queisser limit [8,9].

As a powerful and clean tool for modulating the crystal structure, hydrostatic pressure can be applied to gradually tune the optical and electronic properties of the $MAPbI_3$ perovskites. There have been many experimental studies on the electronic structures and optical properties of $MAPbI_3$ under pressures [10-14]. For example, by applying appropriate hydrostatic pressure, Kong et al. [13] found that a mild pressure can not only narrow down the band gap for broader solar spectrum absorption, but also prolong the carrier lifetime for greater photovoltage in the perovskites, both of which are highly desirable for achieving better photovoltaic performance. More recently, Jaffe et al. studied the pressure effect on the electronic and optical properties of $MAPbX_3$ experimentally and found the metallization of $MAPbI_3$ through apparent band gap closure at pressures above 60 GPa [10,14].

As it is commonly accepted that there is a strong correlation between the structure and properties in the perovskite materials [15,16], in this paper, we systematically study the pressure-induced atomic and electronic structure evolution of $MAPbI_3$ in the cubic perovskite structure using first-principlescalculations. To analyze the mechanism of the pressure induced changes, we have performed detailed studies of the PbI_6 octahedron tilts, Bader analysis, and electronic structure of $MAPbI_3$ under different pressures. Our results demonstrate that the band tuning in the cubic $MAPbI_3$ structure under pressure is the result of the competition between PbI_6 octahedral tilt and lattice contraction. Under moderate pressure, the band gap of $MAPbI_3$ can potentially reach the optimized value of 1.3–1.4 eV, i.e. the Shockley-Queisser limit.

2. Model and computation methods

The first-principles calculations were performed using VASP code [17,18] with the standard frozen-core projector augmented-wave (PAW) method, with the exchange-correlation functional of generalized gradient approximation (GGA) in the Perdew, Burke, and Ernzerhof (PBE) format [19]. Although most of DFT-GGA calculations show underestimated band gaps in various semiconducting materials, quite a peculiar situation seems to exist for the Pb-based perovskites. The DFT-GGA calculated band gaps of the $MAPbI_3$ perovskites are in good consistent with previously 1.53 eV values [4,20]. This is mainly due to the strong relativistic effect of the Pb atoms offsetting the underestimation error of the band gap by the typical GGA calculation. Similar results have also been reported in other Pb-containing materials [21]. Considering that calculations using the GGA-DFT and HSE-SOC methods result in nearly the same band edge orbital characters and band gap positions in k-space, as well as the same trend of the band gap change, GGA-DFT is able to qualitatively provide a correct picture of the electronic structure evolution in $MAPbI_3$ under pressure. Since we mainly focus on the pressure induced electronic band gap evolution, the DFT-GGA calculations were used throughout our studies for total energy and band gap calculation. For the effective mass calculation, we use the screened hybrid functionals of Heyd Scuseria Ernzerhof (HSE) (with α=0.43) including the spin-orbit coupling

(SOC) effects. The vaspkit toolkit code has been used to calculate the effective mass in our calculation [22].

All the $MAPbI_3$ structures under pressures were relaxed until all forces are smaller than 0.01 eV/Å and the structural relaxations were performed with a Gaussian broadening of 0.05 eV. The cut-off energy of 500 eV for basic functions was used in the calculations. A reciprocal space sampling with shift grid of 7×7×7 Monkhorst-Pack mesh [23] of the Brillouin zone was used in the structural optimizations. We note that dispersive interactions have been reported to be essential for accurately describing the structural properties of $MAPbI_3$ and led to lattice constants in better agreement with experiment [24-29]. For example, the lattice constant will be overestimated 2% from 6.35 Å to 6.48 Å without of dispersive interactions [27]. However, this small difference does not affect much the band properties, e.g., neither the band edge orbital characters nor band gap position in k-space have changes. Therefore, although the dispersive interactions were ignored in the current study, our conclusions remain reliable.

$MAPbX_3$ has a cubic perovskite ABX_3 structure with space group Pm-3m (Fig. 1a) at high temperature and high pressure [30,31]. Since the MA is a polar organic cation, its orientations in $MAPbX_3$ have noticeable influence on the structure characteristics such as total energy, crystal lattice and band gap of the system [21,32]. In order to make clear the favorite orientation of the MA cation at zero temperature, we performed the first-principles total energy calculations on various MA orientations using DFT. Three local minima were identified, where the MA dipole is aligned along the <111>, <110>, and <100> directions, respectively. The total energy difference among them is within 40 meV per atom, with the <111> orientation being the most stable one, which is consistent with the results of Giorgi et al. [33]. As shown in Fig. 1, the MA cation in the ground state is surrounded by PbI_6 octahedra and oriented in the <111> direction with the maximum freedom.

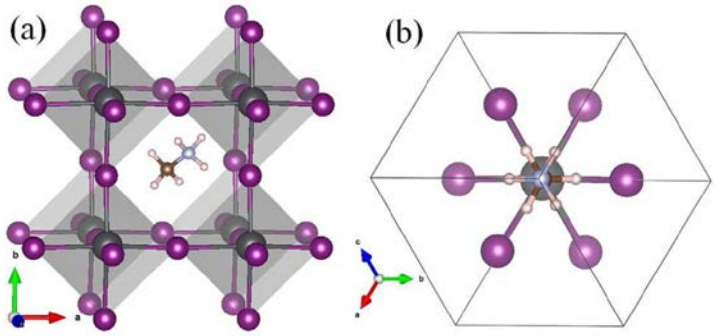

Fig. 1. (a) The schematic polyhedral view of perovskite structure of $MAPbI_3$. (b) The ball and stick view of $MAPbI_3$ along <111> direction.

3. Results and discussion

3.1. Electronic structure of Pm-3m MAPbI3 under ambient pressure

The lattice parameters, band gap and electron/hole mass of the cubic $MAPbI_3$ structure at ambient condition from our calculations are listed in Table 1. In the cubic MAPbI3 structure, MA and Pb donate one and two electrons respectively to three I ions, forming a band gap of 1.593/1.541 eV in DFT-GGA/HSE-SOC between unoccupied Pb 6p orbital and occupied I 5p orbital based on our calculations, consistent with the previous theoretical results [20,21]. The cubic MAPbI3 structure is calculated to be a direct band gap semiconductor with the conduction band minimum (CBM) and the valence band maximum (VBM) at the same R (0.5 0.5 0.5) point. Noticeable density peaks of the MA cation are only found deep in the valence band at −5.5 eV and −9.5 eV below the Fermi level, which barely overlap with the I 5p/Pb 6s orbitals, indicating that there is no significant interaction between the MA cation and Pb/I [20]. The contribution of the MA cation to the band structure near the Fermi level is relatively weak. But as a charge compensation center, the MA cation donates one electron to Pb-I framework.

Table 1. Calculated lattice constant a, band gap energy E_g, effective electron/hole mass of cubic $MAPbI_3$ under ambient pressure. Corresponding results from the references are also presented for comparison.

Methods	*a* (Å)	Eg (eV)	electron mass (m_0)	hole mass (m_0)
DFT-GGA	6.477	1.593	0.298	0.275
HSE-SOC	6.477	1.541	0.197	0.242
DFT-GGA [4]	6.39	1.53		
DFT-GGA [21]	6.33	1.57		
GGA-PBE [33]		1.64	0.32	0.36
GGA-SOC [33]		1.64	0.23	0.29
SR-DFT [34]		1.68	0.36	0.40
GW-SOC [34]		1.67	0.22	0.16
Experiment	6.31 [31]	1.55 [1]		

The remarkable properties of the $MAPbI_3$ perovskite in solar cells benefit partially from its excellent charge transport capacity. Using the parabolic approximation, we calculated effective mass (m*) of carriers around the CBM and the VBM via the fitting of the dispersion relation: $m^*=\hbar^2/[\partial^2E(k)/\partial k^2]$, where E(k) is the band edge eigenvalue and k is the wavevector. The effective electron and hole masses (m_e^* and m_h^*) in the cubic $MAPbI_3$ under ambient pressure are calculated to be 0.298 m_0, and 0.275 m_0, respectively. If the spin-orbit coupling effects are included with HSE the screened hybrid functionals, the value will be 0.197 m_0, and 0.242 m_0, respectively. These are consistent with the results of Giorgi [33] and Umari [34], as shown in Table 1. According to the carrier mobility formula $\mu=qt/m^*$ (where m* is the effective mass of the carrier, q is the elementary charge and t is the average scattering time) [35], it can be seen that smaller effective masses of electron and hole carriers result in faster diffusion rate of

carriers, thus high battery conductivity, which will facilitate the separation and transport of carriers.

3.2. Electronic structure of Pm-3m $MAPbI_3$ under high pressure

By gradually varying the lattice parameter, the cubic $MAPbI_3$ structure was optimized to obtain the relation between total energy and volume of the system. Pressure can then be calculated using $P=-\partial E/\partial V$. Through the first-principles band structure calculations, band gaps under different pressures were computed and plotted in Fig. 2. Here the R-R gap shows the energy gap calculated from the difference between valence maximum and conduction minimum at the high-symmetry R point in the Brillouin zone. The band edge gap represents the energy difference between the valence edge and conduction edge in the total density of states.

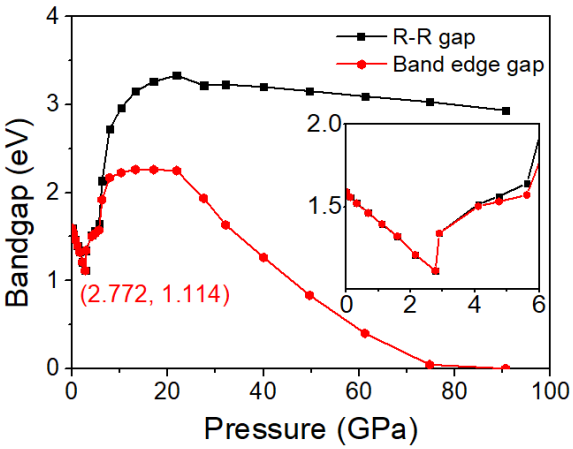

Fig. 2. Variation of the band gap under pressures. Both the gaps calculated at the high symmetry point R and between the band edges are plotted. Inset shows an enlarged plot of the band gap at pressures from 0 to 6 GPa.

At ambient pressure, the band gap has been calculated to be 1.593 eV or 1.541 eV in DFT-GGA or HSE-SOC. As the pressure increases from 0 to 2.772 GPa, it undergoes a redshift to 1.114/1.380 eV in DFT-GGA/HSE-SOC. This means the band gap of the cubic MAPbI3 perovskite can potentially reach the optimized value of 1.3–1.4 eV, i.e. the Shockley-Queisser limit, at which the energy-conversion efficiency of solar cells is the highest. We also note that the effective masses (m_e^* and m_h^*) in $MAPbI_3$ at 2.772 GPa were calculated to be 0.301 m_0 and 0.229 m_0 in DFT-GGA, while it would be 0.171 m_0 and 0.227 m_0 in HSE-SOC calculation, respectively. This decrease in band gap and effective mass comes from the pressure induced coupling change in the band edge states and indicates better charge transport properties as a photovoltaic absorber in the compressed cubic $MAPbI_3$ perovskite.

Continuously increasing the pressure, the band gap will widen again after 2.772 GPa as plotted in Fig. 2. We note that in our calculations the cubic symmetry of the structure is kept. Nonetheless, such variation of the band gap under pressures in $MAPbI_3$ is rather unusual. Applying hydrostatic pressure on a crystal usually narrows its band gap in the absence of phase transitions.

The reason is that the lattice contraction increases the orbital overlap and an easier electronic hopping is allowed when atoms approach each other. However in the cubic $MAPbI_3$ structure, the blueshift of the band gap is observed in the pressure range of 2.772 GPa–20 GPa. More interestingly, at the same time, the CBM starts to shift away from the high symmetry point R and the direct band gap changes to indirect band gap, as shown in the insert plot of Fig. 2. This can also be seen more clearly in Fig. 3a.

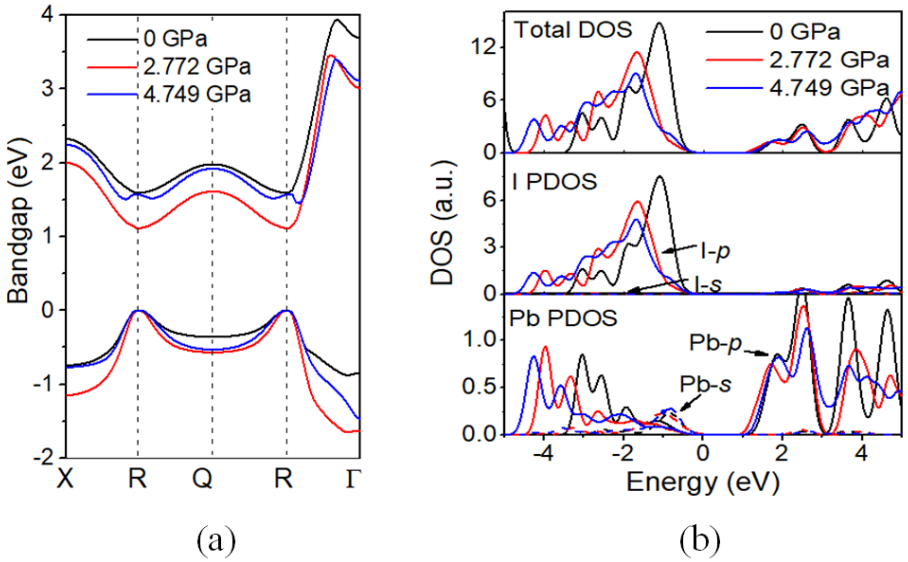

Fig. 3. The electronic structures of the perovskites MAPbI3 under 0, 2.772, and 4.749 GPa pressures. (a) The band edge states near Fermi level. (b) The total DOS and partial I, Pb DOS.

In Fig. 3, we plot the band edge structures and DOS information of $MAPbI_3$under the three selected mild pressures. It shows clearly a redshift and subsequent blue jump below and upon 2.772 GPa. Above of this critical point, the VBM is still at R point, while the CBM shifts away from R point and moves to R-Γ line. This direct-indirect transition relate closely to the polar MA molecular and structure changes in $MAPbI_3$ under pressure and will be discussed in another work [36].

Further increasing the pressure to above 20 GPa, the band gap decreases again as shown in Fig. 2. The $MAPbI_3$ is observed to be metallic at about 80 GPa, not far away from the experimentally reported 60 GPa [14].

3.3. Correlation between the atomic and electronic structure changes

Evolution of the electronic properties of materials under pressure is determined by the changes in its atomic structure. Compared with the ideal cubic $MAPbI_3$ perovskite structure plotted in Fig. 1a, the pressure-driven $MAPbI_3$ exhibits notable rotations of PbI_6 octahedra along with the reduction of Pb-I bond length.

In mild pressure, the octahedral tilt can be seen as a rigid rotation of the anion [PbI6]4− cage with either in-phase or out-of-phase ordering [37,38], resulting in the transformation of the rectangular cavity in which the MA cation sits into an irregular polyhedrons-shaped cavity. It stabilizes the structure primarily because of the nonbonding I 5p orbitals, while the Pb 6s/I 5p bonding states reduce the propensity to such tilt in Pb-based perovskites [38]. At the microscopic level, it was also reported that the hydrogen bonding between the MA cation and the halide frame plays an important role in the octahedral tilting [39].

In order to examine the mechanism of the octahedral tilts, in Fig. 4 we plotted the structures under three different pressures as well as the average Pb-I-Pb angle and relevant bond length parameter C as the function of pressure. C=(b−a/2)/(a/2) is the relevant bond length parameter, where b is the average bond length of Pb-I bonds in $MAPbI_3$ and a is the lattice constant at different pressures. It serves as a good indicator to the tilting level of the PbI_6 octrahedra. At mild pressure (see Fig. 4b), the dominant structure change is observed as the hydrogen atoms attached to the nitrogen end of the MA cation (H_N) approaching to I atoms of the $[PbI_6]^{4-}$ inorganic cage. The change of HN-I distance is due to the attractive Coulomb interaction between H_N and I atoms. This electrostatic in nature and attractive Coulomb interaction between the H_N and halogenatoms have been identified by theory in $MAPbBr_3$ [40] and lead to deviations of the predominant Pb I-Pb bond angle away from 180° (see Fig. 4a–c). Here we note that not all of the HN-I distance becomes shorter with the amine end of the MA molecule towards I atoms due to the asymmetry of MA molecular and disordered cavity.

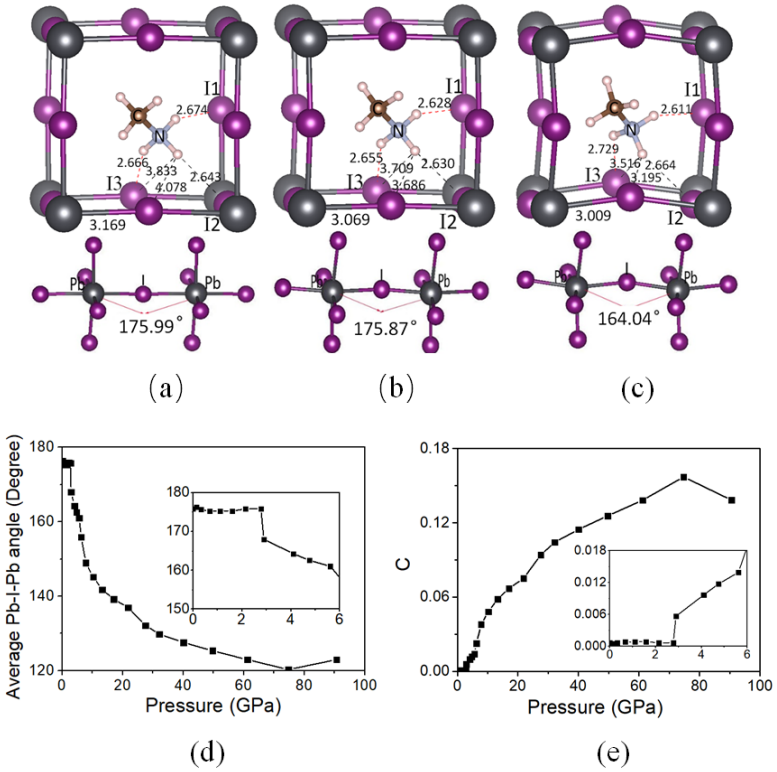

Fig. 4. The HN-I bond lengths in $MAPbI_3$ (upper panel, in the unit of Å.) and the predominant Pb-I-Pb bond angle (lower panel) at (a) 0 GPa, (b) 2.772 GPa, and (c) 4.749 GPa, respectively.

(d) The average angle of Pb-I-Pb in $MAPbI_3$ at different pressures. (e) The relevant Pb-I bond length parameter C at different pressures. Inset plots show the average bond angles and the relevant bond lengths parameter at pressures from 0 to 6 GPa.

To reveal the electronic nature of PbI_6 octahedra rotation, we performed the Bader analysis under different pressures based on the first-principles calculations. The results of the charge transfer are shown in Table 2, where the involved atoms are labeled in Fig. 4. We can see that the charges transferred to N atom are 1.838, 1.852, and 1.891 electrons at 0, 2.772, and 4.749 GPa, respectively. This leaves the H_N atoms with a net positive charge, which in turn get attracted to the negatively charged I atoms. Finally the amine end of the MA cation is driven towards to the I atoms of inorganic cage. At the same time, I atoms of the cage are displaced from their edge centered positions in the ideal cubic perovskite and move towards to the H_N atoms through rotation of PbI_6 octahedra. We plot in Fig. 5 charge density difference at 2.772 GPa between the self-consistent charge density and non-self-consistent superposition of atomic charge density to show how the charge redistributes when the bonds are created. As a qualitative description, the charge density difference plot intuitively shows the bonding or charge aggregation between the atoms due to the charge transfer. From Fig. 5, there are obvious features of covalent bonding between N-H, C-H, and C-N. Apparently the charge aggregations between the shortest three HN-I imply the electrostatic attractive Coulomb interaction between the H_N and halogen atoms, further supporting the mechanism of the rotations of PbI_6 octahedra are highly correlated with the strength of the hydrogen bonding [41].

Table 2. The charge transfer of the H, N and I atoms under three different pressures. The unit of all numbers is e^-.

	H_N	H_N	H_N	**N**	**C**	I_1	I_2	I_3
0 GPa	−0.679	−0.656	−0.712	+1.838	−0.824	+0.464	+0.461	+0.437
2.772 GPa	−0.657	−0.701	−0.681	+1.852	−0.784	+0.407	+0.397	+0.400
4.749 GPa	−0.691	−0.682	−0.674	+1.891	−0.825	+0.405	+0.398	+0.402

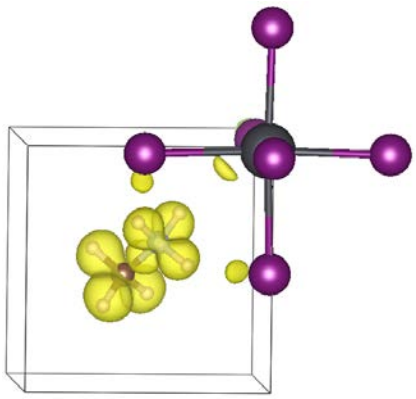

Fig. 5. The charge density difference at 2.772 GPa between the self-consistent charge density and non-self-consistent superposition of atomic charge density of $MAPbI_3$.

Finally, we analyze the relation between the band gap changes and the structure. In Fig. 4d, we notice that Pb-I-Pb bond angle remains almost unchanged below 3 GPa. The band gap decreases in $MAPbI_3$ mainly because the lattice contraction increases Pb-I orbital overlap. At about 2.8 GPa, there is an abrupt change in the Pb-I-Pb bond angle as shown in the inset of Fig. 4d. The Pb-I-Pb bond angle decrease continually in company with the rotation of the PbI6 octahedra (see Fig. 4e). Together with the variation of band gap plotted in Fig. 2, we conclude that the blueshift of the band gap between 2.8 GPa and 20 GPa is caused by the octahedral tilts of PbI_6, which reduces the Pb-I orbital overlap. The two competing effects, i.e. lattice contraction and octahedral tilting, determine the pressure-driven evolution of the band gap for $MAPbI_3$. Above 20 GPa, as the Pb-I-Pb angle decreases slower and the lattice contraction becomes dominate, the band gap starts to decrease and reaches 0 at about 80 GPa according to our calculations.

4. Conclusions

In summary, we investigated the electronic structure evolution of the cubic phase of $MAPbI_3$ perovskite under pressure. It is found that the band gapof the compressed cubic $MAPbI_3$ firstly exhibits a notable redshift and subsequently blue jump under pressure up to ~20 GPa. Upon further increase of the pressure, $MAPbI_3$ eventually becomes metallic at ~80 GPa. It is demonstrated that rotation of PbI_6 octahedra and lattice contraction driven by pressure determine the electronic structure evolution in $MAPbI_3$. The two competing effects have impact on the electronic properties of $MAPbI_3$ through tuning the metal-halide orbital overlaps, where lattice contraction decreases the band gap and octahedral tilting tends to increase the band gap. Although we only considered the cubic phase of $MAPbI_3$ perovskites in this work, rich and unusual pressure induced behaviors are observed in the electronic properties of $MAPbI_3$. These unique electronic properties come from the intricacy of the organic-inorganic trihalide $MAPbI_3$ perovskites and can be transferred to understanding of other organic-inorganic trihalide perovskites.

Acknowledgements

This work is supported by the National Natural Science Foundation of China(Grant No. 11504332) and Outstanding Young Talent Research Fund of Zhengzhou University (Grant No. 1521317008). Work at Ames Laboratory was supported by the U.S. Department of Energy (DOE), Office of Science, Basic Energy Sciences, Materials Science and Engineering Division. Ames Laboratory is operated for the U.S. DOE by Iowa State University under contract #DE-AC02-07CH11358. The calculations were performed on the High Performance Computational Center of Zhengzhou University.

References

[1] A. Kojima, K. Teshima, Y. Shirai, T. Miyasaka, Organometal halide perovskites as visible-light sensitizers for photovoltaic cells, J. Am. Chem. Soc. 131 (17) (2009) 6050–6051, https://doi.org/10.1021/ja809598r.

[2] N.R.E. Laboratory, Research cell efficiency records,

https://www.nrel.gov/pv/ assets/pdfs/pv-efficiencies-07-17-2018.pdf, (October, 2018).

[3] W.-J. Yin, T. Shi, Y. Yan, Unique properties of halide perovskites as possible origins of the superior solar cell performance, Adv. Mater. 26 (27) (2014) 4653–4658, https://doi.org/10.1002/adma.201306281.

[4] W.-J. Yin, J.-H. Yang, J. Kang, Y. Yan, S.-H. Wei, Halide perovskite materials for solar cells: a theoretical review, J. Mater. Chem. A 3 (17) (2015) 8926–8942, https://doi.org/10.1039/C4TA05033A.

[5] A.M.A. Leguy, J.M. Frost, A.P. McMahon, V.G. Sakai, W. Kockelmann, C. Law, X. Li, F. Foglia, A. Walsh, B.C. O'Regan, J. Nelson, J.T. Cabral, P.R.F. Barnes, The dynamics of methylammonium ions in hybrid organicinorganic perovskite solar cells, Nat. Commun. 6 (1) (2015) 7124, https://doi.org/10.1038/ncomms8124.

[6] T. Wang, B. Daiber, J.M. Frost, S.A. Mann, E.C. Garnett, A. Walsh, B. Ehrler, Indirect to direct bandgap transition in methylammonium lead halide perovskite, Energy Environ. Sci. 10 (2) (2017) 509–515, https://doi.org/10.1039/C6EE03474H.

[7] E.M. Hutter, M.C. Gélvez-Rueda, A. Osherov, V. Bulović, F.C. Grozema, S.D. Stranks, T.J. Savenije, Direct-indirect character of the bandgap in methylammonium lead iodide perovskite, Nat. Mater. 16 (1) (2017) 115–120, https://doi.org/10.1038/nmat4765.

[8] W.E.I. Sha, X. Ren, L. Chen, W.C.H. Choy, The efficiency limit of CH 3 NH 3 PbI 3 perovskite solar cells, Appl. Phys. Lett. 106 (22) (2015) 221104, https://doi.org/10.1063/1.4922150.

[9] W. Shockley, H.J. Queisser, Detailed balance limit of efficiency of p-n junction solar cells, J. Appl. Phys. 32 (3) (1961) 510–519, https://doi.org/10.1063/1.1736034.

[10] A. Jaffe, Y. Lin, C.M. Beavers, J. Voss, W.L. Mao, H.I. Karunadasa, High-pressure single-crystal structures of 3D lead-halide hybrid perovskites and pressure effects on their electronic and optical properties, ACS Cent. Sci. 2 (4) (2016) 201–209, https://doi.org/10.1021/acscentsci.6b00055.

[11] Y. Wang, X. Lü, W. Yang, T. Wen, L. Yang, X. Ren, L. Wang, Z. Lin, Y. Zhao, Pressure-induced phase transformation, reversible amorphization, and anomalous visible light response in organolead bromide perovskite, J. Am. Chem. Soc. 137 (34) (2015) 11144–11149, https://doi.org/10.1021/jacs.5b06346.

[12] T. Ou, J. Yan, C. Xiao, W. Shen, C. Liu, X. Liu, Y. Han, Y. Ma, C. Gao, Visible light response, electrical transport, and amorphization in compressed organolead iodine perovskites, Nanoscale 8 (22) (2016) 11426–11431, https://doi.org/10.1039/C5NR07842C.

[13] L. Kong, G. Liu, J. Gong, Q. Hu, R.D. Schaller, P. Dera, D. Zhang, Z. Liu, W. Yang, K. Zhu, Y. Tang, C. Wang, S.-H. Wei, T. Xu, H.-k. Mao, Simultaneous band-gap narrowing and carrier-lifetime prolongation of organicinorganic trihalide perovskites, Proc. Natl. Acad. Sci. 113 (32) (2016) 8910–8915, https://doi.org/10.1073/pnas.1609030113.

[14] A. Jaffe, Y. Lin, W.L. Mao, H.I. Karunadasa, Pressure-induced metallization of the halide perovskite (CH3NH3)PbI3, J. Am. Chem. Soc. 139 (12) (2017) 4330–4333, https://doi.org/10.1021/jacs.7b01162.

[15] M.R. Filip, G.E. Eperon, H.J. Snaith, F. Giustino, Steric engineering of metal-halide perovskites with tunable optical band gaps, Nat. Commun. 5 (2014) 1–9, https://doi.org/10.1038/ncomms6757.

[16] J. Young, J.M. Rondinelli, Octahedral rotation preferences in perovskite iodides and bromides, J. Phys. Chem. Lett. 7 (5) (2016) 918–922, https://doi.org/10.1021/acs.jpclett.6b00094.

[17] G. Kresse, J. Furthmüller, Efficient iterative schemes for ab initio total-energy calculations using a plane-wave basis set, Phys. Rev. B 54 (16) (1996) 11169–11186, https://doi.org/10.1103/PhysRevB.54.11169.

[18] G. Kresse, J. Furthmüller, Efficiency of ab-initio total energy calculations for metals and semiconductors using a plane-wave basis set, Comput. Mater. Sci. 6 (1) (1996) 15–50, https://doi.org/10.1016/0927-0256(96)00008-0.

[19] J.P. Perdew, K. Burke, M. Ernzerhof, Generalized gradient approximation made simple, Phys. Rev. Lett. 77 (18) (1996) 3865–3868, https://doi.org/10.1103/PhysRevLett.77.3865.

[20] W.-j. Yin, T. Shi, Y. Yan, W.-j. Yin, T. Shi, Y. Yan, Unusual defect physics in CH3NH3PbI3 perovskite solar cell absorber, Appl. Phys. Lett. 104 (2014), https://doi.org/10.1063/1.4864778 (2015) 063903.

[21] E. Mosconi, A. Amat, M.K. Nazeeruddin, M. Grätzel, F. De Angelis, First-principles modeling of mixed halide organometal perovskites for photovoltaic applications, J. Phys. Chem. C 117 (27) (2013) 13902–13913, https://doi.org/10.1021/jp4048659.

[22] V. Wang, N. Xu, vaspkit, A pre- and post-processing program for the vasp code https://sourceforge.net/projects/vaspkit/, (2018).

[23] H.J. Monkhorst, J.D. Pack, Special points for Brillouin-zone integrations, Phys. Rev. B 13 (12) (1976) 5188–5192, https://doi.org/10.1103/PhysRevB.13.5188.

[24] Y. Wang, T. Gould, J.F. Dobson, H. Zhang, H. Yang, X. Yao, H. Zhao, Density functional theory analysis of structural and electronic properties of orthorhombic perovskite CH3NH3PbI3, Phys. Chem. Chem. Phys. 16 (4) (2014) 1424–1429, https://doi.org/10.1039/c3cp54479f.

[25] J. Li, P. Rinke, Atomic structure of metal-halide perovskites from first principles: the chicken-and-egg paradox of the organic-inorganic interaction, Phys. Rev. B 94 (4) (2016) 1–12, https://doi.org/10.1103/PhysRevB.94.045201.

[26] X. Zeng, T. Zhou, C. Leng, Z. Zang, M. Wang, W. Hu, X. Tang, S. Lu, L. Fang, M. Zhou, Performance improvement of perovskite solar cells by employing a CdSe quantum dot/PCBM composite as an electron transport layer, J. Mater. Chem. A 5 (33) (2017) 17499–17505, https://doi.org/10.1039/c7ta00203c.

[27] D.A. Egger, L. Kronik, Role of dispersive interactions in determining structural properties of organic-inorganic halide perovskites: insights from first-principles calculations, J. Phys. Chem. Lett. 5 (15) (2014) 2728–2733, https://doi.org/10.1021/jz5012934.

[28] J. Feng, Mechanical properties of hybrid organic-inorganic CH3NH 3BX3 (B = Sn, Pb; X = Br, I) perovskites for solar cell absorbers, Apl. Mater. 2 (8) (2014) 1–8, https://doi.org/10.1063/1.4885256.

[29] J. Endres, D.A. Egger, M. Kulbak, R.A. Kerner, L. Zhao, S.H. Silver, G. Hodes, B.P. Rand, D. Cahen, L. Kronik, A. Kahn, Valence and conduction band densities of states of metal halide perovskites: a combined experimental-theoretical study, J. Phys. Chem. Lett. 7 (14) (2016) 2722–2729, https://doi.org/10.1021/acs.jpclett.6b00946.

[30] Y. Kawamura, H. Mashiyama, K. Hasebe, Structural study on CubicTetragonal transition of CH3NH3PbI3, J. Phys. Soc. Japan 71 (7) (2002) 1694–1697, https://doi.org/10.1143/JPSJ.71.1694.

[31] C.C. Stoumpos, C.D. Malliakas, M.G. Kanatzidis, Semiconducting tin and lead iodide perovskites with organic cations: phase transitions, high mobilities, and near-infrared photoluminescent properties, Inorg. Chem. 52 (15) (2013) 9019–9038, https://doi.org/10.1021/ic401215x.

[32] F. Brivio, A.B. Walker, A. Walsh, Structural and electronic properties of hybrid perovskites for high-efficiency thin-film photovoltaics from first-principles, Apl. Mater. 1 (4) (2013) 042111, https://doi.org/10.1063/1.4824147.

[33] G. Giorgi, J.I. Fujisawa, H. Segawa, K. Yamashita, Small photocarrier effective masses featuring ambipolar transport in methylammonium lead iodide perovskite: a density functional analysis, J. Phys. Chem. Lett. 4 (24) (2013) 4213–4216, https://doi.org/10.1021/jz4023865.

[34] P. Umari, E. Mosconi, F. De Angelis, Relativistic GW calculations on CH3 NH3 PbI 3 and CH3 NH3 SnI3 perovskites for solar cell applications, Sci. Rep. 4 (2014) 1–7, https://doi.org/10.1038/srep04467.

[35] J. Xi, M. Long, L. Tang, D. Wang, Z. Shuai, First-principles prediction of charge mobility in carbon and organic nanomaterials, Nanoscale 4 (15) (2012) 4348, https://doi.org/10.1039/c2nr30585b.

[36] Y. Huang, L. Wang, Z. Ma, F. Wang, Pressure induced band structure evolution of halide perovskites: a first-principles atomic and electronic structure study, J. Phys. Chem. C 123 (1) (2019) 739–745, https://doi.org/10.1021/acs.jpcc.8b11500.

[37] R.J. Angel, J. Zhao, N.L. Ross, General rules for predicting phase transitions in perovskites due to octahedral tilting, Phys. Rev. Lett. 95 (2) (2005) 10–13, https://doi.org/10.1103/PhysRevLett.95.025503.

[38] M.W. Lufaso, P.M. Woodward, Jahn-Teller distortions, cation ordering and octahedral tilting in perovskites, Acta Crystallogr. Sect. B Struct. Sci. 60 (1) (2004) 10–20, https://doi.org/10.1107/S0108768103026661.

[39] J.H. Lee, N.C. Bristowe, J.H. Lee, S.H. Lee, P.D. Bristowe, A.K. Cheetham, H.M. Jang, Resolving the physical origin of octahedral tilting in halide perovskites, Chem. Mater. 28 (12) (2016) 4259–4266, https://doi.org/10.1021/acs.chemmater.6b00968.

[40] S. Sarkar, P. Mahadevan, Role of the A-site cation in determining the properties of the hybrid perovskite CH3NH3PbI3, Phys. Rev. B 95 (21) (2017) 214118, https://doi.org/10.1103/PhysRevB.95.214118.

[41] J.H. Lee, N.C. Bristowe, P.D. Bristowe, A.K. Cheetham, Role of hydrogen-bonding and its interplay with octahedral tilting in CH3NH3PbI3, Chem. Commun. 51 (29) (2015) 6434–6437, https://doi.org/10.1039/C5CC00979K.